Optimizing Raman spectral collection for quartz and zircon crystals for elastic thermobarometry

MAYARA F. CIZINA¹, T. DYLAN MIKESELL¹, AND MATTHEW J. KOHN^{1,*}

¹Department of Geosciences, Boise State University, Boise, Idaho 83725, U.S.A.

ABSTRACT

Raman spectroscopy is widely used to identify mineral and fluid inclusions in host crystals, as well as to calculate pressure-temperature (P-T) conditions with mineral inclusion elastic thermobarometry, for example quartz-in-garnet barometry (QuiG) and zircon-in-garnet thermometry (ZiG). For thermobarometric applications, P-T precision and accuracy depend crucially on the reproducibility of Raman peak position measurements. In this study, we monitored long-term instrument stability and varied analytical parameters to quantify peak position reproducibility for Raman spectra from quartz and zircon inclusions and reference crystals. Our ultimate goal was to determine the reproducibility of calculated inclusion pressures (" P_{inc} ") and entrapment pressures (" P_{trap} ") or temperatures (" P_{trap} ") by quantifying diverse analytical errors, as well as to identify optimal measurement conditions and provide a baseline for interlaboratory comparisons. Most tests emphasized 442 nm (blue) and 532 nm (green) laser sources, although repeated analysis of a quartz inclusion in garnet additionally used a 632.8 nm (red) laser. Power density was varied from <1 to >100 mW and acquisition time from 3 to 270s. A correction is proposed to suppress interference on the ~206 cm⁻¹ peak in quartz spectra by a broad nearby (~220 cm⁻¹) peak in garnet spectra.

Rapid peak drift up to 1 cm⁻¹/h occurred after powering the laser source, followed by minimal drift (<0.2 cm⁻¹/h) for several hours thereafter. However, abrupt shifts in peak positions as large as 2–3 cm⁻¹ sometimes occurred within periods of minutes, commonly either positively or negatively correlated to changes in room temperature. An external Hg-emission line (fluorescent light) can be observed in spectra collected with the green laser and shows highly correlated but attenuated directional shifts compared to quartz and zircon peaks. Varying power density and acquisition time did not affect Raman peak positions of either quartz or zircon grains, possibly because power densities at the levels of inclusions were low. However, some zircon inclusions were damaged at higher power levels of the blue laser source, likely because of laser-induced heating.

Using a combination of 1, 2, or 3 peak positions for the ~128, ~206, and ~464 cm⁻¹ peaks in quartz to calculate P_{inc} and P_{trap} showed that use of the blue laser source results in the most reproducible P_{trap} values for all methods (0.59 to 0.68 GPa at an assumed temperature of 450 °C), with precisions for a single method as small as ± 0.03 GPa (2 σ). Using the green and red lasers, some methods of calculating P_{trap} produce nearly identical estimates as the blue laser with similarly good precision (± 0.02 GPa for green laser, ± 0.03 GPa for red laser). However, using 1- and 2-peak methods to calculate P_{trap} can yield values that range from 0.52 ± 0.06 to 0.93 ± 0.16 GPa for the green laser, and 0.53 ± 0.08 GPa to 1.00 ± 0.45 GPa for the red laser. Semiquantitative calculations for zircon, assuming a typical error of ± 0.25 cm⁻¹ in the position of the ~1008 cm⁻¹ peak, imply reproducibility in temperature (at an assumed pressure) of approximately ± 65 °C.

For optimal applications to elastic thermobarometry, analysts should: (1) delay data collection approximately one hour after laser startup, or leave lasers on; (2) collect a Hg-emission line simultaneously with Raman spectra when using a green laser to correct for externally induced shifts in peak positions; (3) correct for garnet interference on the quartz 206 cm^{-1} peak; and either (4a) use a short wavelength (blue) laser for quartz and zircon crystals for P-T calculations, but use very low-laser power (<12 mW) to avoid overheating and damage or (4b) use either the intermediate wavelength (green; quartz and zircon) or long wavelength (red; zircon) laser for P-T calculations, but restrict calculations to specific methods. Implementation of our recommendations should optimize reproducibility for elastic geothermobarometry, especially QuiG barometry and ZiG thermometry.

Keywords: Raman spectroscopy, elastic thermobarometry, garnet, quartz, zircon

Introduction

Raman spectroscopy on micro-inclusions ("Raman micro-spectroscopy") is widely used to identify organic and inorganic molecules. Raman microspectroscopy can be advantageous because analysis is rapid and, in many cases, causes no damage to a sample.

Raman microspectroscopy is of growing interest for geologic studies (e.g., see review of Chou and Wang 2017), such as to identify minerals (e.g., Korsakov et al. 2010; Nasdala and Schmidt 2020), characterize melts and fluid inclusions (e.g., Rosasco et al. 1975; Mernagh and Wilde 1989; Bodnar and Frezzotti 2020) and determine pressure and temperature (*P-T*) of metamorphic mineral formation using mineral inclusions (e.g., Sobolev and Shatsky

^{*} E-mail: mattkohn@boisestate.edu. Orcid 0000-0002-7202-4525

1990; Beyssac et al. 2002; Enami et al. 2007; Korsakov et al. 2020).

Peak position resolution of 1–2 cm⁻¹ is normally sufficient for mineral identification (Nasdala and Schmidt 2020), or to calculate the integrated area under certain Raman peaks (e.g., for thermometry using carbonaceous materials; Beyssac et al. 2002). However, when using mineral inclusions for elastic geothermobarometry, such as the quartz-in-garnet barometer ("QuiG"-Kohn 2013), calculations are based on precise peak offsets between inclusion and reference crystals. Fortunately, systematic errors such as instrument calibration propagate uniformly across a spectrum, so normally peak position offsets are retained irrespective of exact peak positions. Thus, assessing computational accuracy of *P-T* calculations requires understanding how consistently peak positions and differences in peak positions can be measured.

Machine stability and spectral parameters, including laser source, power density, acquisition time, and number of gratings principally determine the precision of peak positions in Raman spectra. While research in biology and materials science has sought to optimize analytical parameters (e.g., Wahadoszamen et al. 2015; Kerr et al. 2015), little effort has been published on ways to optimize measurements for geologic samples. Most published literature does not document in detail how analytical procedures or external laboratory conditions affect Raman peak positions or *P-T* calculations.

In this study, to serve as a baseline for interlaboratory comparisons and to assess the effects of different approaches on data quality and *P-T* estimates, we conducted a series of experiments (Online Materials¹ Table S1) to quantify the stability of Raman peak positions for reference crystals and inclusions of quartz and zircon, as well as for a Hg atomic-emission line from fluorescent lights (Izraeli et al. 1999). Specifically, we report:

- Long-term stability of peak positions, using sequential ~ 30 s measurements for up to ~ 30 h.
- The effects of varying power and acquisition times on peak positions to identify whether integrated laser flux affects spectra (e.g., through laser-induced heating).
- The effects of different laser sources (wavelengths) on peak stability and signal intensity.

We also characterize the reproducibility of calculated entrapment pressures (at an assumed temperature) based on repeated inclusion-standard measurements using different laser sources and computational methods, as well as a rough calculation of uncertainties in temperature (at an assumed pressure). Last, we compile recommendations for data monitoring and reporting. Overall, machine stability and peak drift (up to 2.5 cm^{-1}) can affect calculated P-T conditions in natural rocks by as much as 0.2–0.4 GPa (for incautious approaches), but optimization of analysis can improve reproducibility to $\pm 0.03 \text{ to } \pm 0.07 \text{ GPa}$ (2σ).

BACKGROUND

Mineral inclusion elastic thermobarometry

Mineral inclusion elastic thermobarometry using Raman microspectroscopy complements classical thermobarometric methods because it does not rely on chemical equilibration of mineral assemblages. Instead, it assumes mechanical equilibrium (e.g., no differential stress at the time of mineral entrapment) and relies on the *P-T* dependence of mineral volumes, i.e., each mineral's compressibility and thermal expansivity. The most commonly

applied elastic barometer today is QuiG (e.g., Enami et al. 2007; Ashley et al. 2014; Spear et al. 2014; Castro and Spear 2017; Murri et al. 2018; Bonazzi et al. 2019; Gonzalez et al. 2019; Alvaro et al. 2020; Spear and Wolfe 2020; Wolfe and Spear 2020; Wolfe et al. 2021; Zuza et al. 2022), while zircon-in-garnet ("ZiG") appears useful as a thermometer (Kohn 2014, 2016; Zhong et al. 2019; Cisneros and Befus 2020; Ehlers et al. 2022).

When an inclusion becomes entrapped in a host crystal, the inclusion and host both experience the same P-T condition, and the void space in the host exactly matches the volume of the inclusion. However, as the rock cools and exhumes to the surface, the inclusion and host will attempt to achieve different volumes because they have different thermoelastic properties (Rosenfeld and Chase 1961). Commonly, quartz inclusions will attempt to expand against surrounding garnet, leading to compression (negative volume strain or "positive pressure"). In some low-P, high-T cases, quartz inclusions will attempt to shrink relative to the surrounding garnet, leading to expansion (positive volume strain or "negative pressure"). By correlating compression or expansion to pressure, the community commonly refers to an inclusion pressure, or " $P_{\rm inc}$ " although there is no way to measure pressure directly, only strain.

Assuming strain has accumulated only elastically post-entrapment, not by flow or fracture, the current strain on an inclusion permits calculation of its entrapment P-T conditions. Angel et al. (2017) proposed a computational approach that employs the concept of an isomeke (Adams et al. 1975a). An isomeke is a curve in P-T space where both the host void space and inclusion have the same change in fractional volume (Adams et al. 1975a; Angel et al. 2014). Because the fractional volumes are the same, the pressure experienced by host and inclusion are the same. This condition fulfills a key assumption of mechanical equilibrium. The theory and computational methods of Angel et al. (2017) allow entrapment pressure (" P_{trap} ") or temperature (" T_{trap} ") to be quantified. Raman peak positions in quartz and zircon depend on crystal strain and can be inverted to quantify the strains in the inclusion (Angel et al. 2019: stRAinMAN software). These strains can be converted to the current pressure on the inclusion $(P_{\rm inc}; Gonzalez et al. 2019; Mazzucchelli et al. 2021), and <math>P_{\rm inc}$ can be inverted to obtain the line of potential entrapment conditions (isomeke) of the inclusion during garnet growth (Angel et al. 2014: EosFitPinc software; Mazzucchelli et al. 2021: EntraPT software). For pressure-sensitive mineral pairs like QuiG, pressure is calculated at an assumed temperature of entrapment yielding a barometric line (Rosenfeld and Chase 1961; Adams et al. 1975b; Enami et al. 2007). For temperature-sensitive mineral pairs like ZiG, temperature is calculated at an assumed pressure of entrapment, yielding a thermometric line (Kohn 2014). Measurements on proximal inclusions can yield a single P-T intersection (Kohn 2016; Zhong et al. 2019).

Reports on measurement protocols

Quantifiably reproducing Raman measurements, and consequently $P_{\rm trap}$ or $T_{\rm trap}$ values, requires documentation of analytical procedures as well as laboratory conditions. Many studies document analytical and machine specifications (e.g., microscope model, objective, grating, spot size, etc.), spectral resolution, and the type of calibration used (e.g., Enami et al. 2007). However, few studies describe laboratory conditions (mainly temperature

stability), peak position stability, or the frequency and timing of reference vs. unknown measurements. These parameters ultimately limit uncertainty in $P_{\rm trap}$ and $T_{\rm trap}$. Different approaches to calculate $P_{\rm trap}$ show different sensitivities to peak position uncertainty. Even relatively small shifts to peak positions can cause significant changes to calculated $P_{\rm trap}$ for some methods (see Discussion). Establishing norms for data collection and reporting is needed to quantify uncertainties in P-T estimates and to compare results among different laboratories.

Methods

Samples

Our experiments were performed with reference (stress-free) crystals of Herkimer quartz and Mud Tank zircon, cut perpendicular to the c-axis. Mud Tank zircon was chosen because it is non-metamict (e.g., Murakami et al. 1991; Pidgeon et al. 2011). Thin slices of reference crystals were polished and separately mounted in putty to reduce the potential of stress gradients across the crystals. For experiments performed on inclusions, we used commercially prepared and polished 100 µm thick sections. The sections contain garnets with inclusions of fully entrapped and isolated quartz and zircon. For quartz, we analyzed sample K87–21C (43.678 °N, 72.199 °W), a metapelite from west-central New Hampshire that was metamorphosed during the Acadian Orogeny (Kohn et al. 1992); for zircon, we analyzed sample ZS-B1 (46.016 °N, 7.842 °W), a metamorphosed ophiolite from the Zermatt-Saas region, Western Alps, formed during the Alpine Orogeny and kindly provided by S. Penniston-Dorland.

Naming convention for peak positions

Peak positions in Raman spectra are commonly referred to using a typical measured peak position, for example, the so-called "464 cm $^{-1}$ " peak in quartz corresponds to the A₁ vibrational mode. However, peak positions for a characteristic Raman band can vary with time or between lasers by more than 1 cm $^{-1}$. In this study, the "464 cm $^{-1}$ " peak was measured at positions ranging from \sim 463 to \sim 467 cm $^{-1}$ depending on day, time of day, or laser source, even when all other analytical conditions were fixed. For simplicity, we refer to the key peaks as 128, 206, and 464 cm $^{-1}$ for quartz (Fig. 1a), 482 cm $^{-1}$ for a Hg atomic-emission line derived from an externally applied fluorescent light (Fig. 1a), and 975 and 1008 cm $^{-1}$ for zircon (Fig. 1b). For many of our data, the actual peak positions are shifted upward systematically by \sim 2 cm $^{-1}$ (possibly reflecting instrument drift after initial calibration on a Si-wafer or repositioning of the diffraction grating post-calibration). Two reference peak positions in garnet occur at \sim 220 and 554 cm $^{-1}$; we use these to correct for garnet interference on the quartz 206 cm $^{-1}$ peak.

Raman measurements

Spectroscopic data were collected with a Horiba Scientific LabRAM HR Evolution at Boise State University in a climate-controlled room following manufacturer specifications. Experiments compared a 532 nm doubled Nd:YAG (green wavelength) with a maximum output power of about 50 mW, and a 442 nm He:Cd (blue wavelength) with a maximum output power of about 120 mW. We emphasize these lasers because they generally produce better count rates and spectra, especially for quartz. Some experiments additionally used a 632.8 nm He:Ne (red wavelength) with a maximum output power of about 17 mW. For simplicity, we refer to these laser sources as "red," "green," and "blue" throughout the rest of this report. Output power was not measured directly and was lower in some measurements (as determined from lower count rates), likely because of drift in alignment. The Raman system is coupled with a thermoelectrically cooled charge-coupled device (CCD) detector (800 mm focal length) with a holographic diffraction grating resolution of 1800 line/mm and a fixed 100 µm aperture size, which gives a confocal (vertical) resolution of roughly 3-4 µm and a channel resolution of 0.3, 0.5, and 0.8 cm⁻¹/pixel for the red, green, and blue lasers, respectively. Note that channel resolution (number of cm-1/pixel) and spectral resolution (ability to separate overlapping peaks) in no way correspond with either peak position resolution or, most importantly, reproducibility of peak positions. Peaks are fitted to multiple points, and even relatively "poor" resolution with the blue laser (0.8 cm⁻¹/channel) typically results in highly precise peak positions (±0.01 cm⁻¹). Conversely, "good" resolution with red or green lasers (0.3 to 0.5 cm⁻¹/channel) cannot always overcome low intensities or peak overlaps. Peak position reproducibility is most important for applications of elastic thermobarometry. This reproducibility can

vary considerably and must be demonstrated for each set of analytical conditions through repeated point measurements or time series experiments.

We calibrated the instrument for all three lasers at the beginning of each day with a mounted Si wafer, and we used quartz and zircon reference crystals to monitor peak position stability continuously over periods of hours to a few tens of hours. We did not attempt to recalibrate the instrument at other times, e.g., after switching lasers. We also monitored green laser stability over hours of Raman spectra collection using a Hg 546.074 nm atomic-emission line derived from an externally applied fluorescent light. The intensity of the line can be adjusted by changing the angle of illumination, distance of the light from the microscope, and magnification lens. We were unable to find cheap, readily available options for use with the red and blue lasers. For all experiments, we used an Olympus 100× objective (<1µm lateral spatial resolution), with a 0.90 numerical aperture and 210 µm working distance. The spectral range used for analyses was between 100 and 600 cm⁻¹ for quartz and 75-1100 cm⁻¹ for zircon. We chose the specified ranges because they have the most relevant peaks for our experiments and can be measured with a minimum of movement of the diffraction grating. Influence of laser power and laser drift was evaluated in reference to the 128, 206, and 464 cm⁻¹ peaks for quartz, the 1008 cm⁻¹ peak in zircon, and (for the green laser), the 482 cm⁻¹ Hg-line (which could be measured using the green laser only).

Raman spectra used to test drift and power density were collected over a small region of a reference grain (about 0.5 by 0.5 $\mu m)$ with either DuoScan imaging or a Marzhauser stage. We used a "scan" rather than point-by-point mode because it was easiest to automate the instrument over periods of hours to tens of hours. We used Neutral Density (ND) filters ranging from 1 to 100% transmission to reduce laser power delivered to the sample. For drift tests, the total acquisition time for each analysis was ~30 s (10 s per acquisition and three accumulations), and for power density tests, from 3 s up to 270 s. Spectra collected at lower power densities had longer acquisition times. For spectra containing the 482 cm $^{-1}$ Hg-line, we used an external light source that was placed adjacent to the microscope. We note that use of a larger microscope objective can allow overhead light to leak into the instrument, potentially providing another source of the 482 cm $^{-1}$ Hg-line.

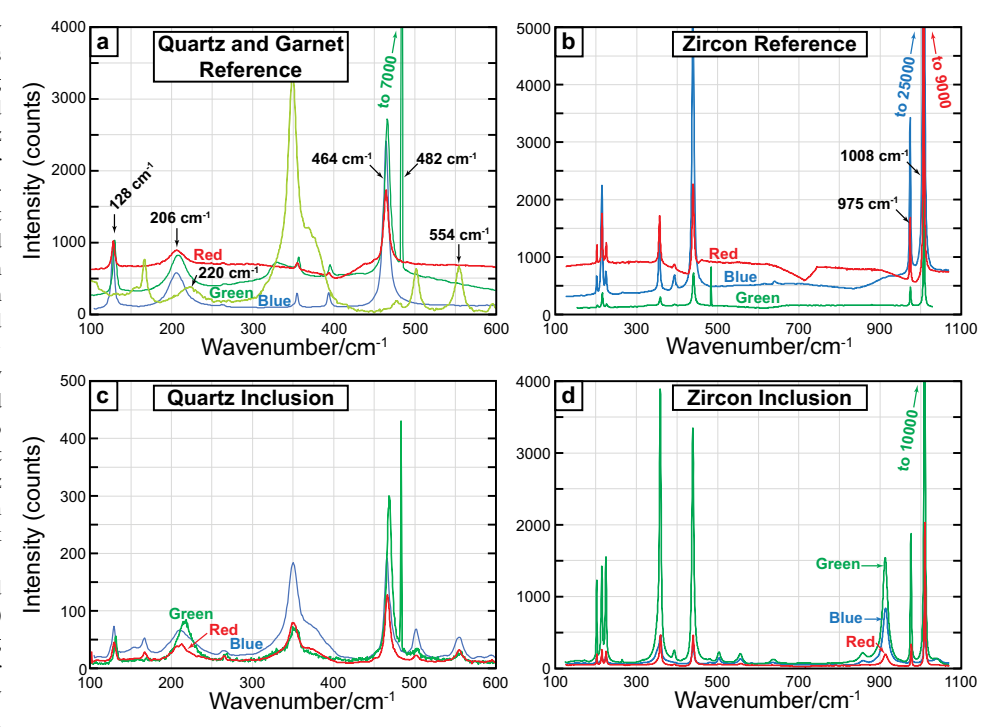
To directly compare results among lasers, we collected spectra on inclusions and reference crystals, cycling among red, green, and blue lasers. In each redgreen-blue cycle, we further alternated measurements between a single inclusion and a reference crystal. Experimental durations were 4 h for quartz and 5 h for zircon (on a different day). The quartz inclusion is $\sim 6.2 \times 3.9 \ \mu m$ in dimension and is located far from any cracks or other inclusions, and $\sim 45 \ \mu m$ from the top surface of the 100 μm thick section. The zircon inclusion is $\sim 6.0 \times 3.9 \ \mu m$ in dimension and is located far from any cracks or other inclusions, and $\sim 52 \ \mu m$ from the top surface of the 100 μm thick section. For each laser, this resulted in 19 measurements for the quartz inclusion, 19 measurements for the reference quartz, 20 measurements for the zircon inclusion, and 20 measurements for the reference zircon. All data were collected during periods of machine stability, and so represent optimal reproducibilities.

Peak fitting

Raman peaks were fit using an in-house MATLAB code based on a nonlinear least-squares curve-fitting method. Each Raman peak was fit using either Gaussian, Lorentzian, or the sum of both functions over specific spectral ranges, as follows:

- (1) An open source function ("baseline") performed automated baseline correction of Raman spectra (Al-Rumaithi 2020).
- (2) The desired spectral range was extracted from the total spectrum and used to define the initial parameters for the fitting routine, which are peak intensity, position, and width. Initial peak intensity was assigned to the maximum value in the extracted spectrum; initial peak position was assigned to the nominal peak position expected in that spectral range (e.g., 128, 206, and 464 cm⁻¹ for quartz; 1008 cm⁻¹ for zircon; 482 cm⁻¹ for Hg-line); peak width at half maximum divided by 2 was calculated and assigned.
- (3) The Curve Fitting toolbox application from MATLAB was applied to generate three different functions: (a) Gaussian, (b) Lorentzian, and (c) sum of Gaussian and Lorentzian (pseudo-Voigt). Each function returned estimated peak positions within the specified range, peak width, and the root mean square error (RMSE) of the fit. All peak positions reported here correspond to the fit function with the lowest RMSE. Differences in peak position fits using our MATLAB code compared to LabSpec 6 (native software for our Raman microscope) and PeakFit (commercial software) are within approximately ±0.02 cm⁻¹ (Online Materials¹ Table S2), which is at or below our level of spot-to-spot reproducibility. We prefer our MATLAB code because it is highly efficient (up to 95 spectral files per minute) and requires less user interaction.

FIGURE 1. Typical raw Raman spectra. Peak positions do not perfectly align among lasers because of drift and systematic offsets. (a) Quartz reference crystal (Herkimer quartz) plus Hg atomicemission line from a fluorescent light (for green laser), and a typical garnet spectrum as measured with the green laser. Quartz peaks labeled 128, 206, 464, and 482 cm⁻¹ were used for reproducibility tests. Garnet peaks labeled 220 and 554 cm⁻¹ were used to correct interference of garnet 220 cm⁻¹ peak on the quartz 206 cm⁻¹ peak. (b) Zircon reference crystal (Mud Tank zircon). Peaks labeled as 975 and 1008 cm-1 were used for reproducibility tests. (c) Quartz inclusion, illustrating low-count rate for red laser (206 cm⁻¹ peak position poorly resolved), and, for green laser,



larger interferences from garnet, but also higher count rates. (d) Zircon inclusion, showing excellent resolution among all lasers. The prominent peak at \sim 910 cm⁻¹ is from garnet. (Color online.)

A slightly modified procedure was applied for fitting the 206 cm⁻¹ peak in quartz inclusion spectra because of interference from a broad ~220 cm⁻¹ garnet peak nearby (Enami 2012). This correction is important for precise calculations because, depending on the quality of the spectrum, corrections to the 206 cm⁻¹ peak position can range up to several cm⁻¹ (Enami 2012). In essence, the contribution of the garnet ~220 cm⁻¹ peak was subtracted from quartz spectra based on shapes and intensities of the ~220 and ~554 cm⁻¹ peaks in reference garnet spectra and on the intensity of the ~554 cm⁻¹ peak in the quartz inclusion spectra. We chose the ~554 cm⁻¹ peak because it is relatively intense, within the 100–600 cm⁻¹ spectral range of interest for quartz, and isolated from other peaks. Raman peak positions for garnets are composition- and pressure-dependent, but the pressure-dependencies for the ~220 and ~554 cm⁻¹ peaks are small [~1.7 and ~2.5 cm⁻¹/GPa vs. ~25 cm⁻¹/GPa for the 206 cm⁻¹ peak in quartz (Gillet et al. 1992; Schmidt and Ziemann 20001). Corrections involved:

- (1) A clean reference spectrum for garnet was collected near the inclusion, and background corrected as above.
- (2) Characteristic garnet peak position, width, and intensity were fit at \sim 220 and \sim 554 cm $^{-1}$. These fitted peaks, not the original spectrum, were used for corrections.
- (3) The quartz inclusion spectrum was background corrected, and the characteristic garnet peak at $\sim\!554~\text{cm}^{-1}$ was fit.
- (4) Counts across the \sim 220 cm⁻¹ peak in the quartz inclusion spectrum were calculated by scaling the \sim 220 cm⁻¹ peak in the garnet spectrum by the peak intensity ratio of the \sim 554 cm⁻¹ peaks in the quartz inclusion spectrum and garnet (corrections for differences in the positions of the \sim 554 cm⁻¹ peaks in the inclusion and reference garnet are negligible and were ignored). These counts were subtracted from the quartz inclusion spectrum.
- (5) The corrected counts in the 206 cm⁻¹ region of the quartz inclusion were fit for the 206 cm⁻¹ peak as above.

Temperature measurements

Laboratory temperature was recorded every 60 s with a CR800 Campbell Scientific datalogger and a Campbell Scientific CS215 temperature and relative humidity probe, with an accuracy of $\pm 0.3^{\circ}$ at 25 °C. The precision of our temperature measurements was ± 0.01 °C ($\pm 2\sigma$), as determined from the reproducibility of measurements collected over short periods of time (tens of minutes). The temperature probe was ~80 cm away from the CCD detector, recording the temperature of the laboratory room. Because each Raman spectrum had a total acquisition

time of \sim 30 s, the temperature and Raman records are offset. Consequently, we used a MATLAB 1-D, cubic spline, interpolation function ("interp1") to correlate temperature and acquisition time.

Entrapment pressure (P_{trap}) calculations

We calculated P_{tmp} for the quartz inclusion in garnet using the peak offsets measured relative to a reference crystal with the three different laser sources. These calculations quantify the reproducibility of calculated P_{tmp} and assess potential differences in calculated P_{tmp} using different laser sources. First, we used our MATLAB code to quantify peak positions for the inclusion and the quartz reference crystal. Then, inclusion-reference peak position differences were calculated directly by simple subtraction. For the green laser, we also tested indirect calculations by subtracting peak position differences relative to the simultaneously measured Hg-line (482 cm⁻¹) peak.

After calculating peak offsets, our preferred approach used the software stRAin-MAN (Angel et al. 2019) to calculate strains in the inclusion, based on offsets for all three 128, 206, and 464 cm⁻¹ peaks. However, the 206 cm⁻¹ peak for the quartz inclusion using the red laser was commonly poorly resolved due to low-count rate and interference with the garnet ~220 cm⁻¹ peak (Fig. 1a). So, we also tested reproducibility using only 2 peak offsets to estimate strain. We then converted strains to average inclusion pressure (Pinc) based on the "elastic tensor method" of Gonzalez et al. (2019) and determined Ptrap values at 450 °C using EosFit-Pinc software with reference equations of state for almandine and quartz (Angel et al. 2017). This approach is equivalent to use of the EntraPT online software (Mazzucchelli et al. 2021). Temperature was chosen as representative of garnet formation in nearby, compositionally similar rocks (Kohn et al. 1992). Use of a different temperature would not change our interpretations. Last, we tested application of simple equations from Kohn (2014) to calculate $P_{\rm inc}$ values with single offsets to the 206 or 464 cm⁻¹ peaks. Calculation for the offset to the 128 cm⁻¹ peak (Δv_{128}) was based on a regression to unpublished experimental data from Schmidt and Ziemann (2000): $P(GPa) = 0.1547\Delta v_{128} + 0.0002722\Delta v_{128}^3$. An analogous expression from Thomas and Spear (2018) has a systematic error of 0.02 to 0.03 GPa because it neglects correction for the peak position at standard temperature and pressure [which was not exactly 128.00 cm⁻¹ in the study of Schmidt and Ziemann (2000)]. It also treats positive strain (expansion) differently from negative strain (contraction). The single-peak approach skips the intermediate step of estimating strains and does not account for stress or strain anisotropy. Last, we used the EosFit-Pinc software (Angel et al. 2017) to calculate P_{trap} from P_{inc} values.

American Mineralogist, vol. 108, 2023

RESULTS

Quality of spectra

In general, any of the three lasers produces acceptable results for reference crystals of quartz and zircon. For quartz (Figs. 1a and 1b), the green and blue lasers produce the highest quality spectra (highest intensities and peak-to-background ratios; Online Materials¹). For quartz inclusions in garnet, data collected using the red laser under typical operating conditions do not always resolve the 206 cm⁻¹ peak (Fig. 1b). For zircon, all three lasers result in highly resolved spectra, but spectra collected with blue and red lasers are superior (Figs. 1c and 1d; Online Materials¹). Spectra for garnet (Fig. 1e) illustrate the potential for overlap of the 206 cm⁻¹ peak and for any peaks between ~300 and ~400 cm⁻¹.

Peak drift

Our day-long stability experiments using the green and blue lasers show several recurring features:

- (1) Initial drift. Within the first ~ 1 h after turning on both laser sources, peak positions drift by as much as ~ 1 cm⁻¹ for both quartz and zircon (hours 0 to 1, Figs. 2a–2d).
- (2) Stabilization. After ~1 h, all Raman spectra show a period up to 5 h of very slow drift (0.01–0.02 cm⁻¹/h; hours 1 to 6, Figs. 2a–2d).
- (3) Other slow drift periods. After the first \sim 5 h, other periods up to several hours long show the slow drift of $<\sim$ 0.05 cm⁻¹/h (e.g., hours 9 to 13, Fig. 2a; hours 14–18, Fig. 2b, etc.). These periods are not necessarily consistent from day to day.
- (4) Abrupt changes. Changes of 0.1 to >2 cm⁻¹ occur at rates ranging from ~ 0.7 to >5 cm⁻¹/h (white labels, Fig. 2). The timing of shifts is not always consistent from day to day, except at $\sim 5:00$ a.m. local time, when the air handling system for the building switched from "night mode" to "day mode." Many shifts also occur near midnight.

- (5) Shifts to peak offsets relative to Hg-line. The difference in the positions of mineral reference peaks relative to the 482 cm⁻¹ Hg-line also shows slow drift and abrupt changes, but the abrupt changes are much smaller in amplitude (<~0.4 cm⁻¹) than in absolute peak position (Figs. 2a and 2c).
- (6) Dependency on room conditions. After moving the instrument to a new building with better power and environmental stability, peak position reproducibility using the green laser improved markedly. The 464 cm⁻¹ peak position and offset relative to 482 cm⁻¹ Hg-line stabilized to ± 0.04 and ± 0.03 cm⁻¹, respectively, 2σ , over a period of 24 h (experiment during March 2022; Online Materials¹ Fig. S1a). The blue laser still shows moderate variability (± 0.18 cm⁻¹, 2σ), which is not ameliorated in reference to the Rayleigh line, but large shifts are reduced to ~ 0.5 cm⁻¹ (Online Materials¹ Fig. S1b).

Temperature correlations

Peak positions commonly correlate negatively with temperature, both in small-scale oscillations (Figs. 3a and 3b) and during larger monotonic shifts (Figs. 3c), but some shifts correlate positively Figs. 3d and 3e). Some rapid peak position shifts also occur while temperature is changing gradually (e.g., between 8 and 10 h, Figs. 2a, 3d, and 3e; at \sim 5 h, Fig. 2c).

Effects of power density and total acquisition time

Varying power density and total acquisition time using the blue or green lasers did not influence peak positions (Fig. 4) or peak width (Online Materials¹) for most types of analysis. Analysis of zircon with varying power using the blue laser (fixed 3 s analytical time) may show a slight down-shift at the highest power. A down-shift would be consistent with heating (e.g., Schmidt et al. 2013). Peak-to-background ratios (Online Materials¹) can show

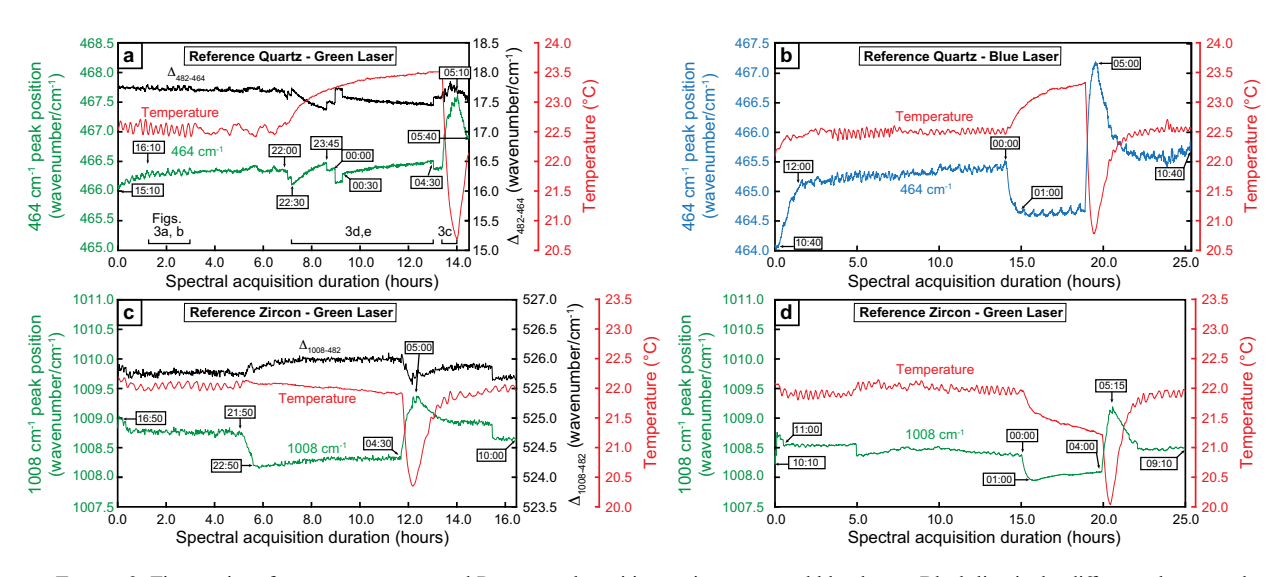


FIGURE 2. Time-series of room temperature and Raman peak positions using green and blue lasers. Black line is the difference between the 482 cm⁻¹ peak (a Hg-line from an external fluorescent light source) and either the 464 cm⁻¹ peak in quartz or the 1008 cm⁻¹ peak in zircon. All time-series are scaled similarly and show initial 0.5–1 cm⁻¹ drift over the first 0.5 to 1.5 h, long periods (several hours) of oscillating but otherwise stable or slowly drifting peak position, and large and rapid shifts in peak positions (bracketing times shown by labels with arrows). (a) Quartz reference crystal, green laser. Labeled black bars refer to regions shown in Figures 3a–3d. (b) Quartz reference crystal, blue laser. (c) Zircon reference crystal, green laser, showing peak shifts at ~22:00 that do not correspond with a temperature shift. (d) Zircon reference crystal, green laser, analyzed on a different day. (Color online.)

increases or decreases with respect to duration of analysis, but these are not systematic, whereas peak-to-background commonly improves with increasing power density. The absence of systematic trends for most data suggests that these power density experiments further quantify peak reproducibility. For both blue and green lasers, during a 1 to 2 h experiment, peak position reproducibility ranges from ± 0.04 to ± 0.21 cm⁻¹ (2σ) for quartz inclusions and ± 0.03 to ± 0.07 cm⁻¹ ($\pm 2\sigma$) for the reference crystal (Figs. 4a and 4b). For zircon, peak position reproducibility ranges from ± 0.09 to ± 0.22 cm⁻¹ (2σ) for inclusions and from ± 0.07 to ± 0.17 cm⁻¹ (2σ) for the reference crystal (Figs. 4c and 4d). This variation is comparable to the reproducibility that we observe for multiple analyses collected on the same material with constant parameters.

Zircon damage using blue excitation wavelength

Massive damage can occur to zircon inclusions when analyzed with the blue laser. In one example at 100% power (nominally 120 mW), a total acquisition time of 3 s did not visibly damage the inclusion (Fig. 5a). Increasing acquisition time to 10 s (with a ND filter of 100%) produced a dark spot in the inclusion

Reference Quartz - Green Lase

482 cm⁻¹ peak position (wavenumber/cm⁻¹)

483.90

(Fig. 5b). A further increase to an acquisition time of 60 s (with a ND filter of 100%) resulted in massive damage to the inclusion and surrounding garnet (Fig. 5c). A few months later, however, we were unable to reproduce the results with the blue laser. We were not able to visibly damage zircon inclusions using the green laser source (50 mW maximum power), even when reproducing the same experimental conditions. Explanations for differences in behavior on different days are considered in the discussion below.

Peak position reproducibility via repeated analysis

Both quartz and zircon inclusions and reference crystals show similar reproducibility of ${\sim}\pm0.2~cm^{-1}~(2\sigma)$ for the 464 and 1008 cm $^{-1}$ peaks as measured via repeated analysis over several hours (Fig. 6). Measurements can be better or poorer for a specific laser source and day. This variation exceeds variability in continuous measurements on the same spot by a factor of ${\sim}2$ (Figs. 2 and 3; Online Materials¹ Table S3). Different lasers also give different absolute peak positions for specific peaks (Fig. 6), probably because of repositioning of the diffraction grating, but peak separations are not statistically different.

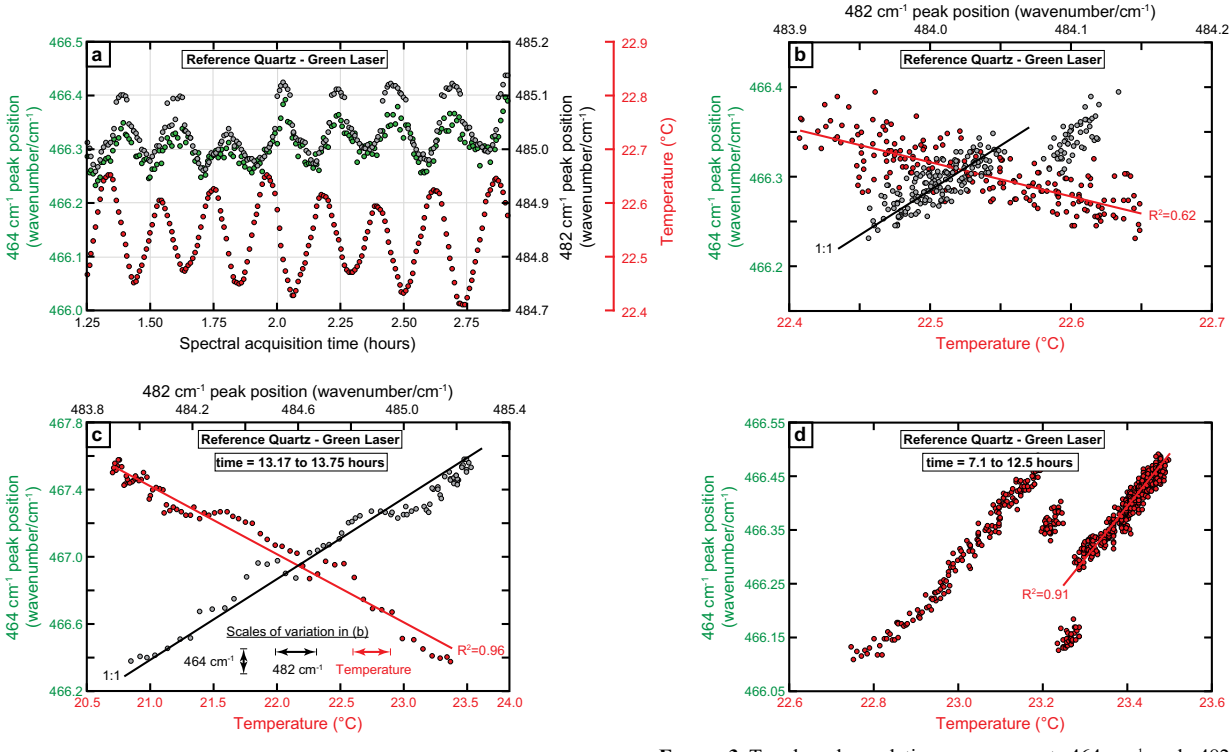


FIGURE 3. Trends and correlations among quartz 464 cm⁻¹ peak, 482 cm⁻¹ peak, and temperature for periods identified in Figure 2. (**a** and **b**) A "stable" period. Small, oscillatory changes in temperature and peak positions strongly correlate with a temporal offset of ~2 min (as determined by cross-correlation; maximum $R^2 = 0.62$). We do not know the cause of the ~0.05 cm⁻¹ jump in 482 cm⁻¹ peak position at ~485.05 cm⁻¹ that degrades an otherwise nearly perfect 1:1 correlation between peak positions. (**c** and **d**) An unstable period. Peak positions sometimes correlate positively with temperature, but may show position jumps between correlated segments. Correlated peak positions may also show deviations from 1:1 line. (**e**) An unstable period. Large, smooth changes in both temperature and peak position correlate closely, although deviations up to ~0.15 cm⁻¹ occur relative to 1:1 line. (Color online.)

American Mineralogist, vol. 108, 2023

483.85

466.5

466.45

466.2

466.05 483.80

464 cm⁻¹ peak position (wavenumber/cm⁻¹)

483.95

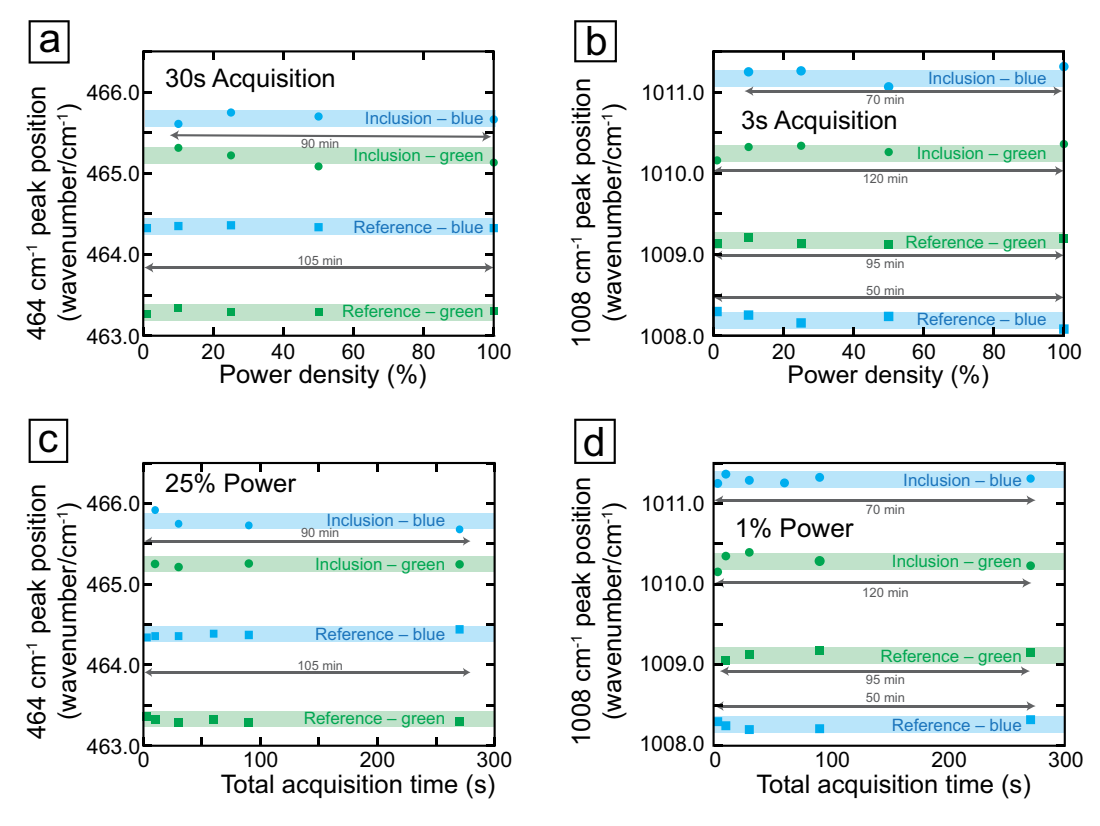


FIGURE 4. Peak positions vs. acquisition time (a and b) and power density (c and d) showing no significant correlations. Colored bands represent ±0.1 cm⁻¹ variation that is typical of best instrument performance during stable periods, and encompass nearly all data. Durations of experiments listed in minutes. Nominal maximum power was 50 mW for green laser and 120 mW for blue laser. Data were collected on different days, so offsets between inclusion vs. reference and between green vs. blue lasers are not meaningful. (a) Quartz 464 cm⁻¹ peak with constant total acquisition time (30 s) and varying ND filters (3–100%). (b) Zircon 1008 cm⁻¹ peak with constant total acquisition time (3 s) and varying ND filters (10–100%). The slight downward trend in peak position for reference crystal, blue laser, could indicate heating. (c) Quartz 464 cm⁻¹ peak with constant ND filter (25%) and varying total acquisition times (3–270 s). (d) Zircon 1008 cm⁻¹ peak with constant ND filter (1%) and varying total acquisition times (3–270 s). Varying power densities and total acquisition times do not obviously affect peak positions. (Color online.)

Apparent entrapment pressures using different lasers

Most calculated $P_{\rm trap}$ values for the single inclusion from sample K87-21C range between 0.60 and 0.67 GPa (Fig. 7; Table 1). Estimates using the single-peak 128 cm⁻¹ method are lower (0.52 to 0.60 GPa), whereas estimates using the two-peak 128–464 cm⁻¹ method are higher (0.67 to 1.00; Fig. 7; Table 1). Kohn et al. (1992) calculated a garnet nucleation pressure of ca. 0.3 GPa at 450 °C for nearby rocks, so all calculated $P_{\rm trap}$ values are much higher than inferred from modeling mineral chemistry. Instead, calculated $P_{\rm trap}$ is much more compatible with rim P-T estimates (ca. 0.7 GPa; Kohn et al. 1992). We do not attempt to interpret this discrepancy but note numerous explanations, including garnet overstepping (e.g., Spear et al. 2014), prograde reequilibration of the inclusion near maximum pressures, and retrograde reequilibration.

Most reproducibilities range from ± 0.03 to ± 0.07 GPa, which is up to 3 times higher than anticipated from minute-to-minute peak reproducibilities during stable times (e.g., Figs. 2, 3a, and 3b). Reproducibility using the 2-peak 128–464 cm⁻¹ method is worst (± 0.16 to ± 0.46 GPa). Excepting the 1-peak 464 cm⁻¹ method, calculations using the red laser data scatter more than for the other two laser sources by a factor of 2–3 (Fig. 7; Table 1).

For data collected with the green laser, referencing peak offsets

to the Hg-line (essentially taking the difference of a difference; Online Materials¹) produces nearly equivalent results as simply subtracting peak positions for inclusion and reference spectra collected as close together in time as possible. Differences in calculated $P_{\rm trap}$ are within 0.01 GPa, except for the 2-peak 128–464 cm⁻¹ method, and reproducibilities are indistinguishable (Table 1).

Summary of peak reproducibility

There are many possible measures of peak position reproducibility, ranging from the precision of numerically fitting a peak position to a measured spectrum, to the variation observed over minutes, hours, or days for a single set of analytical conditions. Some key measures (all errors at $\pm 2\sigma$) for narrow peaks such as at 128, 464, 482, 975, and 1008 cm⁻¹ include:

- (1) Numerical accuracy of our peak fitting routines: ≤±0.02 cm⁻¹, as determined through comparison with other software packages.
- (2) Reproducibility of peak positions and peak position offsets relative to a fixed reference (482 cm⁻¹ Hg line) over periods of minutes to ~ 1 h (short-term stability of instrument): $\pm 0.1-0.2$ cm⁻¹ as determined from continuous time-series measurements of the same analytical spot during periods of stasis or

American Mineralogist, vol. 108, 2023

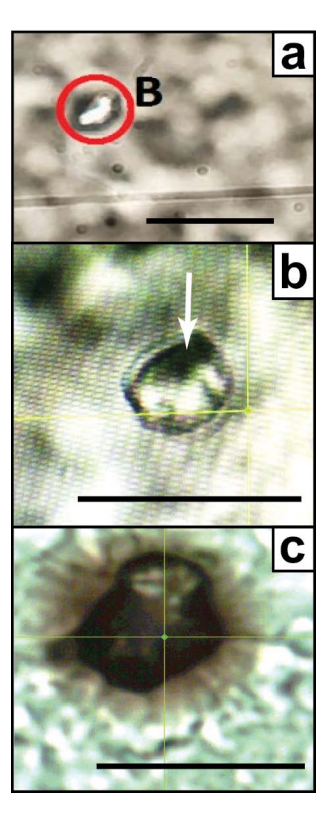


FIGURE 5. Photomicrographs of zircon inclusions in a garnet host, sample ZS-B1. Pictures were taken after Raman spectral acquisition with the 442 nm (blue) laser source. Note that crosshair positions do not always correspond with the analytical location. All scale bars are 20 µm. (a) Undamaged zircon inclusion; high power (100%) and total acquisition time of 3 s. (b) Zircon inclusion with signs of damage (darkening at top of inclusion; arrow); high power (100%) and total acquisition time of 10 s. (c) Highly damaged ("burned") zircon inclusion; high power (100%) and total acquisition time >60 s. (Color online.)

slow drift (Figs. 2 and 3; Online Materials¹ Table S3; improved to ±0.03–0.04 cm⁻¹ in a different room; Online Materials¹ Fig. S1).

- (3) Reproducibility of peak positions over periods of tens of minutes (likely analytical conditions): $\sim \pm 0.2$ cm⁻¹ as determined from tests of the effects of acquisition time and power density on peak positions (Fig. 6) or from repeated cycling of analyses between reference crystal and inclusion (Fig. 7; Online Materials¹ Table S4). Values vary from day to day.
- (4) Reproducibility of peak offsets between sample and reference over periods of tens of minutes (likely analytical conditions): ±0.2 cm⁻¹ (Fig. 6; Online Materials¹ Table S4). Use of the Hg atomic-emission line (taking the difference of a difference) maintains reproducibility (Online Materials¹ Table S4).
- (5) Reproducibility during periods of drift: ±1 cm⁻¹ (Online Materials¹ Table S4) for raw peak positions, but ±0.2 cm⁻¹ when referenced to the Hg atomic-emission line (for green laser).

For use in elastic thermobarometry, the reproducibility of calculated P_{trap} is most relevant: as low as ± 0.03 GPa for the green and blue lasers, but as high as ± 0.4 –0.5 GPa for the red laser, as determined from repeated measurements of reference and sample peak positions (likely analytical conditions; Fig. 7; Table 1).

DISCUSSION

Temporal drift of Raman spectra

Understanding the behavior of instruments and laboratory conditions is critical to optimize Raman data quality and pressure calculations. Peaks initially drift up to 1 cm⁻¹ for approximately one hour after turning on the lasers (Fig. 2). Instrument drift can reflect thermal effects on the instrument, especially the CCD detector, and electric power (Gaufrès et al. 1995; Mestari et al. 1997; Fukura et al. 2006), or physical repositioning of the monochromator. This drift can significantly change some inclusion $P_{\rm trap}$ values, which might then impact geological interpretations. However, the CCD detector in our system is continuously thermoelectrically cooled, even when the lasers are turned off, and the monochromator repositions accurately (to within 0.1 cm⁻¹) when switching between lasers. Stabilization of the lasers, not other components of the instrument, seems most likely responsible for initial drift.

Each laser has its own manufacturer-recommended stabilization period. For our laboratory settings, recommended stabilization times are ~20 min for the blue laser, 1 to 2 min for the green laser, and "a few" minutes for the red laser. If we follow these guidelines, we would obtain erroneous measurements for as much as one hour of initial data collection (Fig. 2). A minimum drift time of 40 min occurs across 20 Raman time series experiments for the green and blue lasers. We did not perform any long-period Raman spectral collection with the red laser, so its long-term stability is unknown. We recommend either waiting for approximately one hour after turning on lasers to start Raman spectral collection, regardless of laser wavelength, or simply leaving the laser power supply turned on.

Well-controlled environmental conditions in the laboratory are essential for precise Raman spectral measurements. In addition to CCD stability, changes in peak position and room temperature can correlate, both during abrupt changes (Figs. 2 and 3) and during small oscillations (Fig. 3; Fukura et al. 2006). Abrupt changes in temperature correlate to the HVAC system in the building, especially late at night, when it changes to "night mode," and 5–6 a.m., when it changes back to "day mode" (Fig. 2). For laboratories that do not maintain temperatures better than ± 0.25 °C over 24 h, we recommend collecting Raman spectra during normal operation hours, when the temperature is most stable. For measurements over longer periods (e.g., 24 h), monitoring temperature may help warn users of potential peak shifts. Changes to ambient temperature do affect peak positions because crystals thermally expand, but typical temperature coefficients are sufficiently small (ca. 0.015–0.03 cm⁻¹/°C; Schmidt and Ziemann 2000; Schmidt et al. 2013) that even the largest changes to room temperature (ca. 3 °C; Fig. 2a) would bias peak positions by <0.1 cm⁻¹.

Temperature is not the only factor influencing instrument stability, however. During at least one time-series experiment, peaks shifted abruptly even as temperature remained nearly constant (Fig. 2c). These shifts may signify changes to electrical systems, potentially correlated with, but independent of, temperature. Thus, even when temperature is well regulated, abrupt shifts to peak positions may occur.

Atomic emission lines (e.g., Hg, Ne) can be used as independent calibrations of strain-induced peak shifts (Online Materials¹ Table S3) and to monitor instrument and spectral stability throughout the

day (Mestari et al. 1997; Izraeli et al. 1999; Hutsebaut et al. 2005; Odake et al. 2008, Jakubek and Fries, 2020; this study). Because the drifts of the Hg-line, quartz, and zircon peaks correlate closely (Fig. 3), light leakage into the microscope (e.g., using a lower magnification lens, e.g., 50× or long working-distance objective) could help monitor and correct for abrupt shifts in Raman peak positions. However, temporal shifts to the Hg, quartz, and zircon lines do not correspond exactly, so their offsets are not identical (e.g., Figs. 2a, 2c, and 3e). Although the changes to offsets between Hg and quartz peaks, and between Hg and zircon peaks are far smaller than individual peak shifts, they can still contribute error on the order of several tenths of a cm⁻¹ (Fig. 2; Online Materials¹ Table S3). This error is similar to, or larger than, typical pointto-point reproducibilities (Figs. 4 and 6). Wherever possible, we recommend using emission lines to monitor machine stability and as a reference for quantitative determinations of peak shifts, but to check reference crystals periodically, especially after any large shifts to absolute positions of emission line spectra. In that context, the green laser may be optimal because commercial fluorescent lights can be used to introduce an external Hg-emission line easily.

Effects of power density and acquisition time on quartz and zircon

Laser absorption can increase the temperature in a sample during analysis and temporarily alter band frequencies and

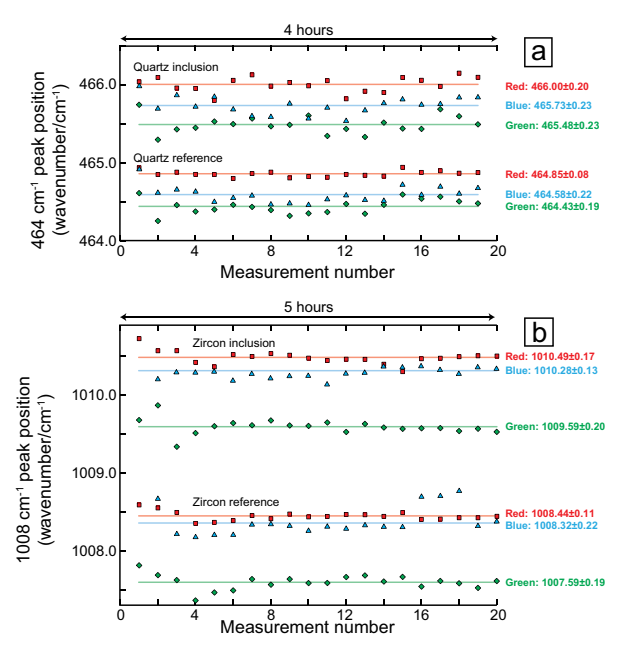


FIGURE 6. Repeated measurements of characteristic peak positions of quartz and zircon inclusion and reference crystals, collected with different wavelength lasers, showing typical reproducibility of ± 0.1 to ± 0.2 cm⁻¹ (2σ) and approximately constant offsets among lasers. Colors of symbols and lines correspond with laser color (excitation wavelength). Values with errors represent mean peak positions with two sigma standard deviations. (a) Quartz 464 cm⁻¹ peak. (b) Zircon 1008 cm⁻¹ peak. The first zircon analysis collected with the blue laser was omitted as an outlier. Differences in absolute peak positions using different lasers could reflect systematic errors arising from repositioning of the grating when switching between lasers. (Color online.)

widths (Nasdala et al. 1998). Constant peak positions (Fig. 4) and peak width (Online Materials¹) indicate that quartz inclusions are not susceptible to heating over wide-ranging power densities (0.5 to 120 mW) and acquisition times (3–270 s). Similarly, we see no evidence for peak shifts in zircon using the green or blue laser (Fig. 4; Online Materials¹). In contrast, peak shifts up to 2 cm⁻¹ at power densities >~10 mW have been reported for zircon analyses collected using the same frequency doubled Nd:YAG (532 nm) laser source (Zhong et al. 2019). The direction of shift is consistent with an increase in temperature during analysis. With the blue laser, discoloration and damage of zircon inclusions at high-power densities (Fig. 5) indicates strong coupling between laser and zircon is possible. If a blue laser is used, we recommend using very low power densities (~12 mW; 10% in our system).

Differences in zircon response to the 532 nm laser in our study vs. Zhong et al. (2019) might reflect differences in depth or prior radiation damage. Zhong et al. (2019) showed a strong heating effect for a relatively shallow zircon inclusion, whereas we analyzed zircons that were far from the sample surface. Attenuation of power with depth might have reduced potential heating in our study. Alternatively, zircons that are more metamict have different bonding structures that shift and broaden Raman peaks and make them more susceptible to light absorption and heating (e.g., Nasdala et al. 1995, 1998; Hoskin and Rodgers 1996; Zhang et al. 2000; Campomenosi et al. 2020). Zircons begin to accumulate α-radiation damage at temperatures below ~230 °C (Pidgeon 2014) similar to the closure temperature of zircon fission tracks (~240 °C; see Bernet and Garver 2005). Our sample from the Alps was metamorphosed at ~40 Ma and cooled through ~240 °C by ~33 Ma (Amato et al. 1999), so radiation damage accumulated for no more than 33 Myr. Values we calculated for FWHM (2–3 cm⁻¹; Online Materials¹) indicate no resolvable radiation damage (Nasdala et al. 2001). In contrast, the rocks that Zhong et al. (2019) analyzed from the Bergen Arcs, Norway, were metamorphosed at 425-430 Ma and cooled below 250 °C by 250-300 Ma (Dunlap and Fossen 1998). While we do not know the U and Th concentration in each zircon inclusion, the magnitude of metamictization of the zircons analyzed by Zhong et al. (2019) was likely many times larger than in our rocks, possibly making the Bergen Arcs zircons more susceptible to laser heating. If so, analysis of young zircons with low degrees of radiation damage, such as in our samples, may permit use of higher laser power or longer acquisition times. Trace elements show a wide range of light absorption characteristics, so differences in trace element contents (e.g., HREE) might also cause differences in heating. Because U and HREE contents vary considerably among zircon crystals, susceptibility to heating must be highly specific to each zircon crystal. Low-power analysis is prudent.

Zircon damage using the blue laser source

The sensitivity of the Raman signal in zircon to the blue laser source (442 nm) allowed us to collect high-quality spectra for inclusions using power densities as low as 1%, and acquisition times as short as 3 s (Fig. 4). However, damage occurred to some zircon inclusions for longer acquisition times or at higher power

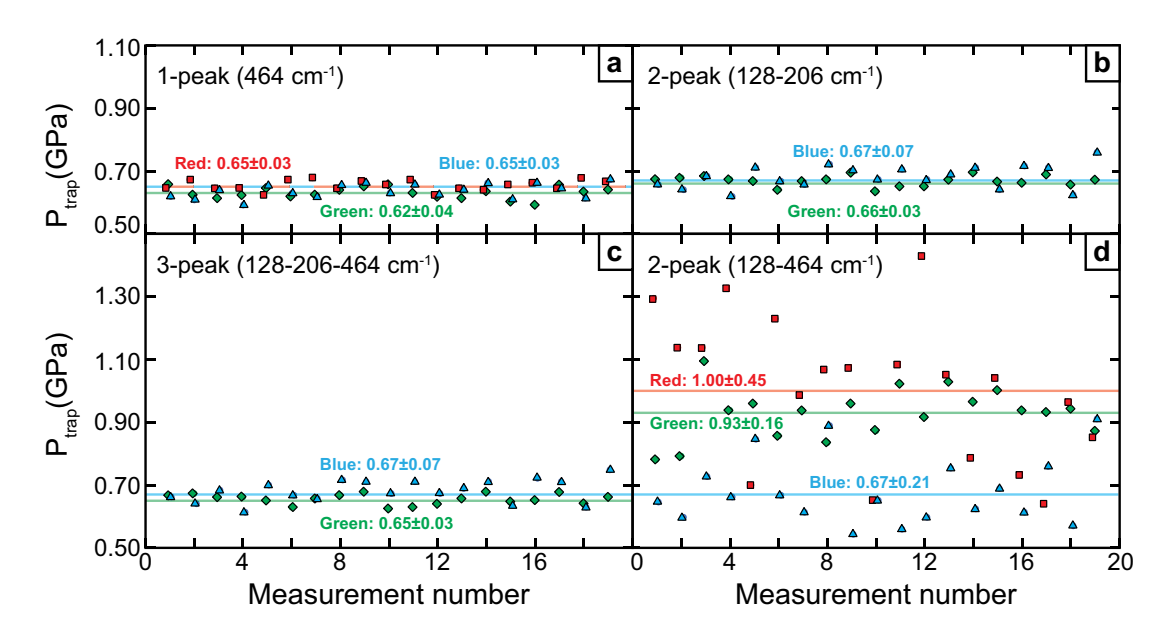


FIGURE 7. Reproducibility of quartz entrapment pressure (P_{trap}) using different methods and laser sources. Symbols have been offset for clarity. Highly reproducible and consistent P_{trap} values between 0.62 and 0.67 GPa occur for (**a**) 1-peak method using 464 cm⁻¹ peak, (**b**) 2-peak strain method using 128 and 206 cm⁻¹ peaks, and (**c**) 3-peak method using 128, 206, and 464 cm⁻¹ peaks. (**d**) 2-peak strain method using 128 and 464 cm⁻¹ peaks yields large scatter, and P_{trap} values for red and green lasers that differ significantly from other methods. (Color online.)

(Fig. 5). Most likely, these zircons absorbed more radiation at 442 nm and consequently heated, even though lower total fluence on other zircons caused no obvious change to peak positions. However, our attempts at more detailed, repeat experiments failed to damage the zircon. This failure could reflect degrading laser alignment or output power, which would reduce the laser flux to the sample, resulting in less heating (if heating is occurring) and a reduced Raman signal. The zircon that shows no heating effects is also relatively deep (\sim 50 μ m below the surface). Lower signal intensity during the repeat experiments is consistent with any of these explanations.

Overall, using shorter excitation wavelengths, such as the blue (442 nm) laser, yields higher Raman scattering intensity, as expected because Raman scattering intensity should scale inversely to the fourth power of the excitation wavelength (McCreery 2000).

TABLE 1. Average P_{trap} calculations ($\pm 2\sigma$) for a single quartz inclusion in garnet

	$P_{\rm trap}$ (blue)	P _{trap} (green)	$P_{\rm trap}$ (red)
1 peak (128)—Quartz reference	0.60 ± 0.05	0.53 ± 0.06	0.53 ± 0.10
1 peak (128)—Hg-line		0.52 ± 0.06	
1 peak (206)—Quartz reference	0.63 ± 0.04	0.60 ± 0.02	
1 peak (206)—Hg line		0.60 ± 0.02	
1 peak (464)—Quartz reference	0.65 ± 0.03	0.63 ± 0.03	0.65 ± 0.03
1 peak (464)—Hg line		0.62 ± 0.04	
2 peaks (128–206)—Quartz reference	0.67 ± 0.07	0.66 ± 0.03	
2 peaks (128–206)—Hg line		0.66 ± 0.03	
2 peaks (128–464)—Quartz reference	0.67 ± 0.21	0.91 ± 0.16	1.00 ± 0.45
2 peaks (128–464)—Hg line		0.93 ± 0.16	
2 peaks (206–464)—Quartz reference	0.67 ± 0.07	0.64 ± 0.04	
2 peaks (206–464)—Hg line		0.64 ± 0.04	
3 peaks—Quartz reference	0.67 ± 0.07	0.65 ± 0.03	
3 peaks—Hg line		0.65 ± 0.03	

Notes: Different combinations of laser sources and Raman peak shifts were used, relative to a quartz reference crystal or a Hg-emission line. Pressure calculated at 450 °C. Spectra collected with the red laser were commonly too poor to permit calculations with the 206 cm⁻¹ peak.

Using the blue laser source to analyze zircon results in faster spectral collection because it covers a wider spectral range, produces higher intensity spectra, and results in higher peak-to-background ratios. However, the laser must be checked a priori to establish which power setting will not irreversibly alter zircon inclusions.

IMPLICATIONS

Optimizing QuiG barometry

For inclusion elastic barometry, calculated P_{trap} can be sensitive to small shifts in Raman peak positions depending on the method used. Consequently, the large abrupt shifts in peaks that we observe due to machine instability (Fig. 2) could be misconstrued to represent significant differences in P_{trap} . An example using the "single peak 464 cm-1" method (e.g., Spear et al. 2014; Zuza et al. 2022) illustrates the concern: consider an inclusion-reference offset of 1.5 cm⁻¹ to the 464 cm⁻¹ peak. This peak shift implies $P_{\rm inc}$ ~0.17 GPa (equation from Kohn 2014) or, at 450 °C, $P_{\rm trap}$ ~0.71 GPa (Angel et al. 2017). If we add a modest abrupt 1 cm⁻¹ peak shift to this offset, $P_{inc} \sim 0.28$ GPa and $P_{trap} \sim 0.89$ GPa, for a difference in apparent of P_{trap} 0.18 GPa. Thus, machine instability can potentially lead to systematic errors in P_{trap} up to 0.1 to 0.2 GPa, at least by this method. These shifts far exceed the reproducibility of the instrument. During times of instrument stability, the single peak 464 cm⁻¹ method yields P_{trap} reproducibilities of ± 0.03 –0.04 GPa for all 3 lasers (Table 1; $\pm 2\sigma$), and identical mean P_{trap} values to within ± 0.015 GPa.

Calculated $P_{\rm trap}$ depends on which laser source and Raman peaks are used. For example, when using a two-peak combination of the 128 and 464 cm⁻¹ peaks, red and green laser sources can yield significantly higher calculated $P_{\rm trap}$ values compared to the blue laser (Fig. 7; Table 1). Apparently, calculated $P_{\rm trap}$ can be sensitive to the omission of the 206 cm⁻¹ mode. The 206 cm⁻¹ peak

cannot always be measured reliably with the red laser, whereas overlap between the 206 cm⁻¹ peak and the garnet ~220 cm⁻¹ peak in spectra collected with the green laser recommends extra correction of the 206 cm⁻¹ peak for interference by the ~220 cm⁻¹. The small variability in calculated $P_{\rm trap}$ values using the blue and green lasers generally reflects well-resolved Raman peaks (high peak-to-background ratio; Online Materials¹). While either laser is excellent for QuiG barometry, other minerals could experience heating (e.g., metamict zircon) or fluorescence (kyanite; Kohn, unpublished data). Thus, it is important to test different laser sources to determine which one optimizes Raman scattering intensities and peak resolution.

Interestingly, use of the 3-peak method to calculate $P_{\rm trap}$ is highly insensitive to systematic shifts in peak positions. For example, typical shifts for the quartz inclusion of 0.5 cm⁻¹ for the 128 cm⁻¹ peak, 3.0 cm⁻¹ for the 206 cm⁻¹ peak, and 1.0 cm⁻¹ for the 464 cm⁻¹ peak (Online Materials¹ Table S4), imply $P_{\rm trap} \sim 0.673$ GPa at 450 °C. Increasing and decreasing all offsets by 1.0 cm⁻¹ increases and decreases calculated $P_{\rm trap}$ to 0.685 and 0.670 GPa, respectively. Changes of ± 0.01 GPa are less than $P_{\rm trap}$ reproducibility (Table 1). We, therefore, advocate use of the 3-peak method of Angel et al. (2017), not only for theoretical reasons but also because it mitigates the effects of systematic errors.

Optimizing ZiG thermometry

We have not performed the same extensive error analysis for ZiG thermometry as for QuiG thermometry because ZiG thermometry additionally requires assessing how metamictization and composition (especially Hf content) affect peak position (Nasdala et al. 1995, 2001; Hoskin and Rodgers 1996). Composition and metamictization may also affect fluorescence and heating of zircon inclusions (Zhong et al. 2019; this study). Nonetheless, any use of zircon spectra for elastic thermobarometry requires identifying optimal analytical conditions. Analytically, the green laser generally produces acceptable spectra but with the lowest intensities, lowest peak-to-background ratios, and largest interferences with garnet compared to the red and blue lasers. The main advantage of the green laser is the potential to add a Hg-emission reference line. Otherwise, the red laser is most reproducible (Online Materials¹ Table S4), while heating with the blue laser cautions extremely short durations or low fluences for data collection.

Implications for prior studies

Although we do not reevaluate all prior studies, most published results are likely accurate in the context of analytical uncertainties, at least within the scope of published interpretations. Recent work that uses the methods of Angel et al. (2014, 2017) and Mazzucchelli et al. (2021) to invert shifts to the 128, 206, and 464 cm⁻¹ peak positions for strain, $P_{\rm inc}$, and $P_{\rm trap}$ (e.g., Gonzalez et al. 2019; Harvey et al. 2021) are highly insensitive to analytical errors. Other studies, with large numbers of data and repeat measurements (e.g., Spear et al. 2014; Viete et al. 2018) or that reference analyses to independent vibrational lines (e.g., Ashley et al. 2014) are likely also robust. Whereas peak shifts might have occurred for some analyses, large data sets are statistically less susceptible to such error. Nonetheless, studies that rely on shifts to a single peak (e.g., Ashley et al. 2014; Spear et al. 2014; Zuza et al. 2022) may warrant reconsideration. Our results may also help explain otherwise

enigmatic observations, for example, variable reproducibility of replicates (Viete et al. 2018) and single outliers (Zuza et al. 2022).

Best practices

Characterizing the reproducibility of Raman spectra of mineral inclusions is essential to achieve optimal P-T calculations in elastic geothermobarometry. Machine instabilities range from small oscillations of \sim 0.1 cm $^{-1}$ (Fig. 3a) to large abrupt shifts >2 cm $^{-1}$ (Fig. 2b) that can compromise accurate P_{trap} values, depending on the methods used. To mitigate these effects, we recommend the following.

- Waiting for approximately one hour after turning on lasers to collect Raman spectra or keeping the lasers on at all times.
- (2) Collecting at least one time-series of spectra on a standard over a period of hours to tens of hours to quantify instrument stability and identify potential for systematic errors.
- (3) Collecting at least one set of sample-reference intercomparisons (Figs. 6 and 7; Online Materials¹ Table S4) and propagating errors (Table 1) or collecting multiple replicates (e.g., Viete et al. 2018) to characterize uncertainties in $P_{\rm inc}$ and $P_{\rm trap}$.
- (4) Using externally imposed emission line spectra (e.g., Hg-line; Izraeli et al. 1999) in addition to a reference crystal to check machine stability and make drift corrections. It is not clear whether "bleed" of the non-scattered laser through the notch filter (Rayleigh line at 0 cm⁻¹) represents an independent reference line because peak position depends on filter efficiency, which may not be uniform. At least one preliminary test cautions against this approach (Online Materials¹ Fig. S1).
- (5) Correcting for the interference of the garnet 220 cm⁻¹ peak on the quartz 206 cm⁻¹ peak through ratioing to isolated garnet peaks (such as the 554 cm⁻¹ peak). This correction is most important for green lasers, where garnet interference is largest (Fig. 1).

In our experiments, varying power density or acquisition time did not induce significant peak shifts for the quartz and zircon inclusions we analyzed using either green or blue lasers, but other zircon inclusions can be susceptible to heating (Zhong et al. 2019; Fig. 5). Depth of the inclusion below the surface, trace element contents, and radiation damage might cause differential laser absorption and heating among zircon grains, so we recommend using relatively low power densities (<~12 mW) with these lasers, especially for inclusions that are close to the section surface. Further studies could focus on what causes damage to zircons using different laser sources.

The blue laser source gives the most consistent results for all methods of estimating $P_{\rm trap}$ (Fig. 7). Use of the red and green laser can yield more precise results, but only for specific methods. We recommend using the elastic tensor approach to invert shifts to the 128, 206, and 464 cm⁻¹ peaks for strain, $P_{\rm inc}$, and $P_{\rm trap}$ (Angel et al. 2014, 2017; Gonzalez et al. 2019; Mazzucchelli et al. 2021), not only because this method is theoretically most robust, but also because it strongly mitigates instrumental errors.

Lastly, in addition to parameters that are commonly reported (e.g., microscope model, objective, grating, focal length, laser type, power, wavelength, confocal aperture diameter, slit size, spectral range and resolution, spot size, acquisition time), we recommend reports include:

- (1) Number of inclusions being analyzed.
- (2) Size and depth of each inclusion (or verification that

- distances from physical boundaries and other inclusions exceed 2-3 grain radii).
 - (3) Frequency of machine calibration.
- (4) Frequency of reference crystal spectral collection. If an external reference is not collected with every spectrum (e.g., Hg-line), we recommend collecting a reference spectrum within 10 min of measuring unknowns to correct for peak drift.
- (5) Peak position reproducibility for all relevant peaks based on spot-to-spot analyses.
 - (6) Propagated reproducibility in P_{inc} .
 - (7) Propagated reproducibility in P_{trap}

ACKNOWLEDGMENTS AND FUNDING

Special thanks are due to Paul Davis for maintaining the Raman microscope and patiently fielding our numerous questions and instrument tests, to Pam Aishlin Cedillo for overseeing temperature measurements in the laboratory, and to S. Penniston-Dorland for providing the Alpine blueschist. We also thank Xin Zhong and an anonymous reviewer for helpful comments, and Sam Couch for providing reference spectra. Supported by a GSA research fellowship to M.F.C., NSF grants EAR1918488 and 1450507 to M.J.K., Boise State University, and a Chinese Academy of Sciences President's International Fellowship to M.J.K.

REFERENCES CITED

- Adams, H.G., Cohen, L.H., and Rosenfeld, J.L. (1975a) Solid inclusion piezothermometry I: Comparison dilatometry. American Mineralogist, 60, 574-583.
- (1975b) Solid inclusion piezothermometry II: Geometric basis, calibration of the association quartz-garnet, and application to some pelitic schists. American Mineralogist, 60, 584-598.
- Al-Rumaithi, A. (2020) Raman spectrum baseline removal. Available: https://www.mathworks.com/matlabcentral/fileexchange/69649-raman-spectrum-baseline-removal) (accessed September 8, 2020). MATLAB Central File Exchange.
- Alvaro, M., Mazzucchelli, M.L., Angel, R.J., Murri, M., Campomenosi, N., Scambelluri, M., Nestola, F., Korsakov, A., Tomilenko, A.A., Marone, F., and others. (2020) Fossil subduction recorded by quartz from the coesite stability field. Geology, 48, 24-28, https://doi.org/10.1130/G46617.1.
- Amato, J.M., Johnson, C.M., Baumgartner, L.P., and Beard, B.L. (1999) Rapid exhumation of the Zermatt-Saas ophiolite deduced from high-precision Sm-Nd and Rb-Sr geochronology. Earth and Planetary Science Letters, 171, 425-438, https://doi.org/ 10.1016/S0012-821X(99)00161-2.
- Angel, R.J., Mazzucchelli, M.L., Alvaro, M., Nimis, P., and Nestola, F. (2014) Geobarometry from host-inclusion systems: The role of elastic relaxation. American Mineralogist, 99, 2146-2149, https://doi.org/10.2138/am-2014-5047.
- Angel, R.J., Mazzucchelli, M.L., Alvaro, M., and Nestola, F. (2017) EosFit-Pinc: A simple GUI for host-inclusion elastic thermobarometry. American Mineralogist, 102, 1957-1960, https://doi.org/10.2138/am-2017-6190.
- Angel, R.J., Murri, M., Mihailova, B., and Alvaro, M. (2019) Stress, strain and Raman shifts. Zeitschrift für Kristallographie. Crystalline Materials, 234, 129-140, https:// doi.org/10.1515/zkri-2018-2112.
- Ashley, K.T., Caddick, M.J., Steele-MacInnis, M.J., Bodnar, R.J., and Dragovic, B. (2014) Geothermobarometric history of subduction recorded by quartz inclusions in garnet. Geochemistry, Geophysics, Geosystems, 15, 350-360, https://doi.org/ 10.1002/2013GC005106
- Bernet, M. and Garver, J.I. (2005) Fission-track analysis of detrital zircon. Reviews in Mineralogy and Geochemistry, 58, 205–237, https://doi.org/10.2138/rmg.2005.58.8.
- Beyssac, O., Goffé, B., Chopin, C., and Rouzaud, J.N. (2002) Raman spectra of carbonaceous material in metasediments: A new geothermometer. Journal of Metamorphic Geology, 20, 859-871, https://doi.org/10.1046/j.1525-1314.2002.00408.x
- Bodnar, R.J. and Frezzotti, M.L. (2020) Microscale chemistry: Raman analysis of fluid and melt inclusions. Elements, 16, 93-98. gselements. 16.2.93.
- Bonazzi, M., Tumiati, S., Thomas, J.B., Angel, R.J., and Alvaro, M. (2019) Assessment of the reliability of elastic geobarometry with quartz inclusions. Lithos, 350-351, 105201, https://doi.org/10.1016/j.lithos.2019.105201.
- Campomenosi, N., Rubatto, D., Hermann, J., Mihailova, B., Scambelluri, M., and Alvaro, M. (2020) Establishing a protocol for the selection of zircon inclusions in garnet for Raman thermobarometry. American Mineralogist, 105, 992-1001, https://doi.org/ 10.2138/am-2020-7246.
- Castro, A.E. and Spear, F.S. (2017) Reaction overstepping and re-evaluation of peak P-T conditions of the blueschist unit Sifnos, Greece: Implications for the Cyclades subduction zone. International Geology Review, 59, 548-562, https://doi.org/ 10.1080/00206814.2016.1200499.
- Chou, I.-M. and Wang, A. (2017) Application of laser Raman micro-analyses to Earth and planetary materials. Journal of Asian Earth Sciences, 145, 309–333, https://doi.org/ 10.1016/j.jseaes.2017.06.032.
- Cisneros, M. and Befus, K.S. (2020) Applications and limitations of elastic thermo-

- barometry: Insights from elastic modeling of inclusion-host pairs and example case studies. Geochemistry, Geophysics, Geosystems, 21, 9231, https://doi.org/ 10.1029/2020GC009231.
- Dunlap, W.J. and Fossen, H. (1998) Early Paleozoic orogenic collapse, tectonic stability, and late Paleozoic continental rifting revealed through thermochronology of K-feldspars, southern Norway. Tectonics, 17, 604-620, https://doi.org/ 10.1029/98TC01603.
- Ehlers, A.M., Zaffiro, G., Angel, R.J., Boffa Ballaran, T., Carpenter, M.A., Alvaro, M., and Ross, N.L. (2022) Thermoelastic properties of zircon: Implications for geothermobarometry. American Mineralogist, 107, 74-81, https://doi.org/10.2138/ am-2021-7731.
- Enami, M. (2012) Influence of garnet hosts on the Raman spectra of quartz inclusions. Journal of Mineralogical and Petrological Sciences, 107, 173-180, https://doi.org/ 10.2465/jmps.111216.
- Enami, M., Nishiyama, T., and Mouri, T. (2007) Laser Raman microspectrometry of metamorphic quartz: A simple method for comparison of metamorphic pressures. American Mineralogist, 92, 1303-1315, https://doi.org/10.2138/am.2007.2438.
- Fukura, S., Mizukami, T., Odake, S., and Kagi, H. (2006) Factors determining the stability, resolution, and precision of a conventional Raman spectrometer. Applied Spectroscopy, 60, 946–950, https://doi.org/10.1366/000370206778062165.
- Gaufrès, R., Huguet, P., and Arab, Y. (1995) Method for the determination of spectral shifts in Raman spectroscopy. Journal of Raman Spectroscopy: JRS, 26, 243-253, https://doi.org/10.1002/jrs.1250260307.
- Gillet, P., Fiquet, G., Malézieux, J.M., and Geiger, C.A. (1992) High-pressure and high-temperature Raman spectroscopy of end-member garnets: pyrope, grossular and andradite. European Journal of Mineralogy, 4, 651-664.
- Gonzalez, J.P., Thomas, J.B., Baldwin, S.L., and Alvaro, M. (2019) Quartz-in-garnet and Ti-in-quartz thermobarometry: Methodology and first application to a quartzofeldspathic gneiss from eastern Papua New Guinea. Journal of Metamorphic Geology, 37, 1193-1208, https://doi.org/10.1111/jmg.12508.
- Harvey, K.M., Penniston-Dorland, S.C., Kohn, M.J., and Piccoli, P.M. (2021) Assessing P-T variability in mélange blocks from the Catalina Schist: Is there differential movement at the subduction interface? Journal of Metamorphic Geology, 39(3), 271-295.
- Hoskin, P.W.O. and Rodgers, K.A. (1996) Raman spectral shift in the isomorphous series (Zr_{1-x}Hf_x)SiO₄. European Journal of Solid State and Inorganic Chemistry, 33, 1111-1121.
- Hutsebaut, D., Vandenabeele, P., and Moens, L. (2005) Evaluation of an accurate calibration and spectral standardization procedure for Raman spectroscopy. The Analyst, 130, 1204-1214, https://doi.org/10.1039/b503624k.
- Izraeli, E.S., Harris, J.W., and Navon, O. (1999) Raman barometry of diamond formation. Earth and Planetary Science Letters, 173(3), 351-360.
- Jakubek, R.S. and Fries, M.D. (2020) Calibration of Raman wavenumber in large Raman images using a mercury-argon lamp. Journal of Raman Spectroscopy: JRS, 51, 1172-1185, https://doi.org/10.1002/jrs.5887.
- Kerr, L.T., Byrne, H.J., and Hennelly, B.M. (2015) Optimal choice of sample substrate and laser wavelength for Raman spectroscopic analysis of biological specimen. Analytical Methods, 7, 5041-5052, https://doi.org/10.1039/C5AY00327J.
- Kohn, M.J. (2013) "Geoba-Raman-try": Calibration of spectroscopic barometers for mineral inclusions. American Geophysical Union, Fall Meeting 2013, V53D-04, https://ui.adsabs.harvard.edu/abs/2013AGUFM.V53D..04K/abstract.
- (2014) "Thermoba-Raman-try": Calibration of spectroscopic barometers and thermometers for mineral inclusions. Earth and Planetary Science Letters, 388, 187-196, https://doi.org/10.1016/j.epsl.2013.11.054.
- (2016) Metamorphic chronology—a tool for all ages: Past achievements and future prospects. American Mineralogist, 101, 25-42, https://doi.org/10.2138/ am-2016-5146.
- Kohn, M.J., Orange, D.L., Spear, F.S., Rumble, D., and Harrison, T.M. (1992) Pressure, temperature, and structural evolution of west-central New Hampshire: Hot thrusts over cold basement. Journal of Petrology, 33, 521-556, https://doi.org/10.1093/ petrology/33.3.521.
- Korsakov, A.V., Perraki, M., Zhukov, V.P., De Gussem, K., Vandenabeele, P., and Tomilenko, A.A. (2010) Is quartz a potential indicator of ultrahigh-pressure metamorphism? Laser Raman spectroscopy of quartz inclusions in ultrahighpressure garnets. European Journal of Mineralogy, 21, 1313-1323, https://doi.org/ 10.1127/0935-1221/2009/0021-2006.
- Korsakov, A.V., Kohn, M.J., and Perraki, M. (2020) Applications of Raman spectroscopy in metamorphic petrology and tectonics. Elements, 16, 105-110, https://doi.org/ 10.2138/gselements.16.2.105.
- Mazzucchelli, M.L., Angel, R.J., and Alvaro, M. (2021) EntraPT: An online platform for elastic geothermobarometry. American Mineralogist, 106, 830-837, https://doi.org/ 10.2138/am-2021-7693CCBYNCND
- McCreery, R.L. (2000) Raman Spectroscopy for Chemical Analysis, 420 p. Wiley. Mernagh, T.P. and Wilde, A.R. (1989) The use of the laser Raman microprobe for the
- determination of salinity in fluid inclusions. Geochimica et Cosmochimica Acta, 53, 765-771, https://doi.org/10.1016/0016-7037(89)90022-7.
- Mestari, A., Gaufrès, R., and Huguet, P. (1997) Behaviour of the calibration of a Raman spectrometer with temperature changes. Journal of Raman Spectroscopy, 28, 785-789, https://doi.org/10.1002/(SICI)1097-4555(199710)28:10<785:AID-JRS148>3.0.CO;2-D.

- Murakami, T., Chakoumakos, B.C., Ewing, R.C., Lumpkin, G.R., and Weber, W.J. (1991)
 Alpha-decay event damage in zircon. American Mineralogist, 76, 1510–1532.
- Murri, M., Mazzucchelli, M.L., Campomenosi, N., Korsakov, A.V., Prencipe, M., Mihailova, B.D., Scambelluri, M., Angel, R.J., and Alvaro, M. (2018) Raman elastic geobarometry for anisotropic mineral inclusions. American Mineralogist, 103, 1869–1872.
- Nasdala, L. and Schmidt, C. (2020) Applications of Raman spectroscopy in mineralogy and geochemistry. Elements, 16, 99–104, https://doi.org/10.2138/ oselements 162 99
- Nasdala, L., Irmer, G., and Wolf, D. (1995) The degree of metamictization in zircon: A Raman spectroscopic study. European Journal of Mineralogy, 7, 471–478, https:// doi.org/10.1127/ejm/7/3/0471.
- Nasdala, L., Pidgeon, R.T., Wolf, D., and Irmer, G. (1998) Metamictization and U-Pb isotopic discordance in single zircons: A combined Raman microprobe and SHRIMP ion probe study. Mineralogy and Petrology, 62, 1–27, https://doi.org/10.1007/BF01173760.
- Nasdala, L., Wenzel, M., Vavra, G., Irmer, G., Wenzel, T., and Kober, B. (2001) Metamictisation of natural zircon: Accumulation versus thermal annealing of radioactivity-induced damage. Contributions to Mineralogy and Petrology, 141, 125–144, https://doi.org/10.1007/s004100000235.
- Odake, S., Fukura, S., and Kagi, H. (2008) High precision in Raman frequency achieved using real-time calibration with a neon emission line: Application to three-dimensional stress mapping observations. Applied Spectroscopy, 62, 1084–1087, https:// doi.org/10.1366/000370208786049169.
- Pidgeon, R.T. (2014) Zircon radiation damage ages. Chemical Geology, 367, 13–22, https://doi.org/10.1016/j.chemgeo.2013.12.010.
- Pidgeon, R.T., Nemchin, A.A., and Kamo, S.L. (2011) Comparison of structures in zircons from lunar and terrestrial impactites. Canadian Journal of Earth Sciences, 48, 107–116, https://doi.org/10.1139/E10-037.
- Rosasco, G.J., Roedder, E., and Simmons, J.H. (1975) Laser-Excited Raman spectroscopy for nondestructive partial analysis of individual phases in fluid inclusions in minerals. Science, 190, 557–560, https://doi.org/10.1126/science.190.4214.557.
- Rosenfeld, J.L. and Chase, A.B. (1961) Pressure and temperature of crystallization from elastic effects around solid inclusions in minerals? American Journal of Science, 259, 519–541, https://doi.org/10.2475/ajs.259.7.519.
- Schmidt, C. and Ziemann, M.A. (2000) In-situ Raman spectroscopy of quartz: A pressure sensor for hydrothermal diamond-anvil cell experiments at elevated temperatures. American Mineralogist, 85, 1725–1734, https://doi.org/10.2138/am-2000-11-1216.
- Schmidt, C., Steele-MacInnis, M., Watenphul, A., and Wilke, M. (2013) Calibration of zircon as a Raman spectroscopic pressure sensor to high temperatures and application to water-silicate melt systems. American Mineralogist, 98, 643–650, https:// doi.org/10.2138/am.2013.4143.
- Sobolev, N.V. and Shatsky, V.S. (1990) Diamond inclusions in garnets from metamorphic rocks: A new environment for diamond formation. Nature, 343, 742–746, https:// doi.org/10.1038/343742a0.
- Spear, F.S. and Wolfe, O.M. (2020) Revaluation of "equilibrium" P-T paths from zoned garnet in light of quartz inclusion in garnet (QuiG) barometry. Lithos, 372–373, 105650, https://doi.org/10.1016/j.lithos.2020.105650.
- Spear, F.S., Thomas, J.B., and Hallett, B.W. (2014) Overstepping the garnet isograd: A

- comparison of QuiG barometry and thermodynamic modeling. Contributions to Mineralogy and Petrology, 168, 1059, https://doi.org/10.1007/s00410-014-1059-6.
- Thomas, J.B. and Spear, F.S. (2018) Experimental study of quartz inclusions in garnet at pressures up to 3.0 GPa: Evaluating validity of the quartz-in-garnet inclusion elastic thermobarometer. Contributions to Mineralogy and Petrology, 173, 42, https:// doi.org/10.1007/s00410-018-1469-y.
- Viete, D.R., Hacker, B.R., Allen, M.B., Seward, G.G.E., Tobin, M.J., Kelley, C.S., Cinque, G., and Duckworth, A.R. (2018) Metamorphic records of multiple seismic cycles during subduction. Science Advances, 4, eaaq0234, https://doi.org/10.1126/ sciadv.aaq0234.
- Wahadoszamen, M., Rahaman, A., Hoque, N.M.R., I Talukder, A., Abedin, K.M., and Haider, A.F.M.Y. (2015) Laser Raman spectroscopy with different excitation sources and extension to surface enhanced Raman spectroscopy. Journal of Spectroscopy, 2015, 895317, https://doi.org/10.1155/2015/895317.
- Wolfe, O.M. and Spear, F.S. (2020) Regional quartz inclusion barometry and comparison with conventional thermobarometry and intersecting isopleths from the Connecticut Valley Trough, Vermont and Massachusetts, U.S.A. Journal of Petrology, 61, egaa076, https://doi.org/10.1093/petrology/egaa076.
- Wolfe, O.M., Spear, F.S., and Harrison, T.M. (2021) Pronounced and rapid exhumation of the Connecticut Valley Trough revealed through quartz in gamet Raman barometry and diffusion modelling of garnet dissolution-reprecipitation reactions. Journal of Metamorphic Geology, 39, 1045–1069, https://doi.org/10.1111/jmg.12601.
- Zhang, M., Salje, E.K.H., Farnan, I., Graeme-Barber, A., Daniel, P., Ewing, R.C., Clark, A.M., and Leroux, H. (2000) Metamictization of zircon: Raman spectroscopic study. Journal of Physics Condensed Matter, 12, 1915–1925, https://doi.org/ 10.1088/0953-8984/12/8/333.
- Zhong, X., Andersen, N.H., Dabrowski, M., and Jamtveit, B. (2019) Zircon and quartz inclusions in garnet used for complementary Raman thermobarometry: Application to the Holsnøy eclogite, Bergen Arcs, Western Norway. Contributions to Mineralogy and Petrology, 174, 50, https://doi.org/10.1007/s00410-019-1584-4.
- Zuza, A.V., Levy, D.A., and Mulligan, S.R. (2022) Geologic field evidence for non-lithostatic overpressure recorded in the North American Cordillera hinterland, northeast Nevada. Geoscience Frontiers, 13, 101099, https://doi.org/10.1016/j.gsf.2020.10.006.

MANUSCRIPT RECEIVED DECEMBER 18, 2021
MANUSCRIPT ACCEPTED MAY 13, 2022
ACCEPTED MANUSCRIPT ONLINE MAY 25, 2022
MANUSCRIPT HANDLED BY CALLUM HETHERINGTON

Endnote:

¹Deposit item AM-23-58423, Online Materials. Deposit items are free to all readers and found on the MSA website, via the specific issue's Table of Contents (go to http://www.minsocam.org/MSA/AmMin/TOC/2023/May2023_data/May2023_data.html).